Article

MPPT Circuit Using Time Exponential Rate Perturbation and Observation for Enhanced Tracking Efficiency for a Wide Resistance Range of Thermoelectric Generator

Jie Miao[12], Houpeng Chen [123*], Yu Lei [12*], Yi Lv[12], Weili Liu[12] and Zhitang Song[12]

[1] State Key Laboratory of Functional Materials for Informatics, Laboratory of Nanotechnology, Shanghai Institute of Microsystem and Information Technology, Chinese Academy of Sciences, Shanghai 200050, China
[2] University of Chinese Academy of Sciences, Beijing 100049, China
[3] Shanghai Technology Development and Entrepreneurship Platform for Neuromorphic and AI SoC, Shanghai 200090, China
* Correspondence: chp6468@mail.sim.ac.cn (H.C.); leiyu@mail.sim.ac.cn(Y.L.)

Abstract: The thermoelectric generator (TEG) stands out in many energy harvesters due to its simple structure, small size, etc. However, previous studies rarely probe into the influence of TEG internal resistances on extracting maximum power from TEG, and tracking efficiency is limited. By analyzing the relationship between the tracking efficiency and the TEG internal resistances, a time exponential rate perturbation and observation (P&O) technology is proposed to achieve maximum power point tracking (MPPT) for a wide resistance range of TEG. Using the time exponential rate P&O, the MPPT circuit observes the power change by comparing PMOS on-time and perturbs the power by adjusting NMOS on-time exponentially. The MPPT circuit is implemented in a 110nm CMOS process. The tracking efficiency keeps a high level from 98.9 to 99.5%. The applicable range of the TEG resistance is from 1 to 12Ω, which is enhanced at least 2.2 times.

Keywords: maximum power point tracking (MPPT), thermoelectric generator (TEG), time exponential rate perturbation and observation (P&O), power modulator

1. Introduction

With the flourish of wearable devices and implantable medical devices, self-powered applications are preferred for avoiding battery replacement or recharging regularly. Therefore, clean and environmentally friendly energy harvesting technology, which scavenges ambient energy, is getting more and more attention due to its super long service life [1-6]. The thermoelectric generator (TEG), which converts thermal energy into electricity based on the Seebeck effect, stands out in many energy harvesters due to its simple structure, small size, rich thermal energy, no pollution, and no noise [7-12].

A TEG is composed of a series of thermocouples (TC) sandwiched between two high-thermal-conductivity substrates. It can be modeled as a DC voltage source E_{TEG} and an internal resistance R_{TEG} connected in series, as shown in Figure 1. According to the Seebeck effect, the E_{TEG} can be expressed as

$$E_{TEG} = N\alpha\Delta T \quad (1)$$

where N is the number of thermocouples, ΔT is the temperature difference between two sides of the TEG, α is the Seebeck coefficient in V/K. α is material-related and not relevant to the size of the thermocouples. The R_{TEG} is mainly determined by the size and the electrical resistivity of the semiconductor materials. Limited by the device area and temperature differences, the E_{TEG} fluctuated in the range of 50-400mV and the R_{TEG} varies from 1Ω to 12Ω in most wearable applications[13,14]. Therefore, extracting as much power as possible is crucial to the converter for TEG.

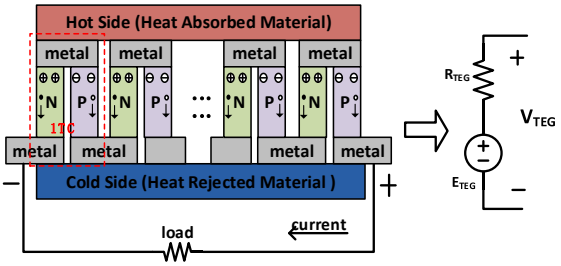

Figure 1. Thermoelectric generator and its equivalent electrical model

Because of the restricted space condition, maximum power point tracking(MPPT) methods for wearable devices usually adopt fractional open circuit voltage (FOCV) [15][16] or perturbation and observation (P&O) [17,18] technique rather than complex algorithms that need to fetch and deal with large amounts of data [19].

According to the TEG electrical model in Figure 1, the maximum output power happens when the TEG output voltage (V_{TEG}) is half of its present open-circuit voltage (E_{TEG}). A converter using the FOCV technique periodically turns off the connection between TEG and boost circuit to sample the TEG open-circuit voltage. During the boost circuit operation, V_{TEG} is automatically tuned around half of E_{TEG} to extract maximum power [20,21]. Although the FOCV technique is simple to implement, it must frequently stop the boost circuit for a while to sample the V_{TEG}, which reduces the system efficiency. To overcome the drawback of the FOCV technique, the P&O technique is proposed for TEG by Rawy [22] and Bandyopadhyay [23]. But the tracking efficiencies fluctuate wildly, especially for a wide R_{TEG} range.

By analyzing the influence of TEG internal resistances on tracking efficiency, a time exponential rate P&O technology is proposed to address the above problems. Using the time exponential rate P&O, the MPPT circuit observes the power by comparing PMOS on-time and perturbs the power by adjusting NMOS on-time exponentially, which shows an enhanced tracking efficiency for a wide R_{TEG} range.

2. Time exponential rate P&O algorithm

Considering the low output voltage of TEG (<400mV), a boost DC-DC converter is used to step up the voltage, as shown in Figure 2. According to the volt-second theory of inductor, the relationship between voltage and on-time of the boost converter is

$$t_{MN} V_{TEG} = t_{MP} (V_{OUT} - V_{TEG}) \quad (2)$$

where V_{OUT} is the output voltage of the boost converter, t_{MN} and t_{MP} are the on-time of the power transistor MN and MP respectively.

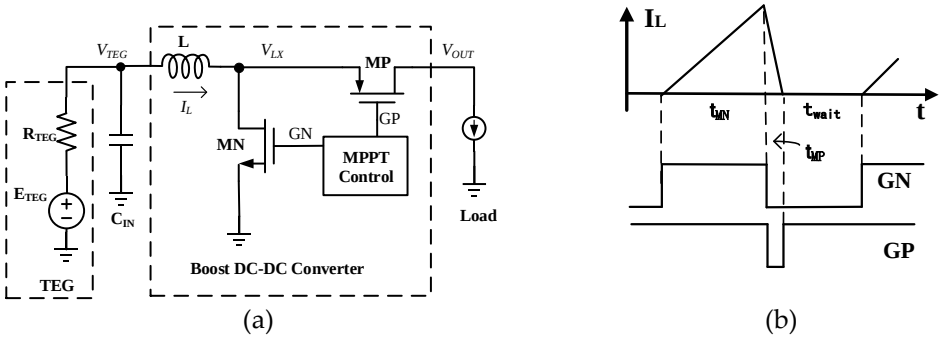

Figure 2. Proposed boost DC-DC converter (a)topology architecture (b) inductor current and control signals

Because of the high conversion rate for this implementation, the inductor current IL declines much faster than it increases and the boost converter works in discontinuous

conduction mode. Accordingly, the average current through the inductance can be expressed as

$$\overline{I_L} = \frac{t_{MN}(t_{MN}+t_{MP})V_{TEG}}{2TL} \tag{3}$$

where L is the inductance, T is the cycle time of the converter. The input power of the converter can be expressed as

$$P_{IN} = V_{TEG} \cdot \overline{I_L} = \frac{V_{TEG}^{\ 2} \cdot t_{MN}(t_{MN}+t_{MP})}{2TL} \tag{4}$$

By substituting Eq. (2) into Eq. (4) and considering the high conversion rate ($V_{OUT} \gg V_{TEG}$), P_{IN} can be approximated to

$$\begin{aligned} P_{IN} &= \frac{V_{TEG}(t_{MN}+t_{MP})\cdot V_{TEG}\, t_{MN}}{2TL} \\ &= \frac{V_{OUT}\, t_{MP}\cdot(V_{OUT}-V_{TEG})\, t_{MP}}{2TL} \approx \frac{V_{OUT}^{\ 2}\cdot t_{MP}^{\ 2}}{2TL} \end{aligned} \tag{5}$$

Observing Eq. (5), we find that the on-time t_{MP} reflects the P_{IN} when the converter works in pulse-width modulation (PWM) mode and output V_{OUT} changes slightly.

As a function of the equivalent resistance of the boost converter (R_{eq}), P_{IN} can be expressed as

$$P_{IN} = \left(\frac{E_{TEG}}{R_{TEG}+R_{eq}}\right)^2 \cdot R_{eq} \tag{6}$$

The P_{IN} reaches the maximum when R_{eq} is equal to R_{TEG}.

According to Eq. (6), tracking efficiency, which is the ratio of input power to ideal maximum input power, can be expressed as

$$\eta_{track} = \frac{P_{IN}}{P_{IN(MAX)}} = \frac{4R_{TEG}\,R_{eq}}{(R_{TEG}+R_{eq})^2} > \varepsilon, \quad 0<\varepsilon<1 \tag{7}$$

where ε is a constant. By rearranging Eq. (7), we can obtain

$$\frac{R_{TEG}}{\beta} < R_{eq} < R_{TEG}\cdot\beta \quad , \quad \beta = \frac{1+\sqrt{1-\varepsilon}}{1-\sqrt{1-\varepsilon}} \tag{8}$$

Consequently, if R_{eq} is in the range of R_{TEG}/β to βR_{TEG}, the tracking efficiency of the MPPT system will remain higher than ε. When $R_{eq}(n)$ is a geometric sequence with a common ratio $\beta^{1/2}$, there are at least three $R_{eq}(n)$ in the range of R_{TEG}/β to βR_{TEG} for arbitrary RTEG, as shown in Figure 3.

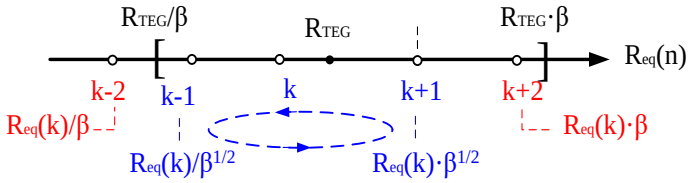

Figure 3. $R_{eq}(n)$ is a geometric sequence with a common ratio $\beta^{1/2}$, and $R_{eq}(k)$ is one of the $R_{eq}(n)$ closest to R_{TEG}.

Figure 4 graphically represents the entire process of the time exponential rate P&O algorithm. In each MPPT cycle, the present t_{MP} is sampled and compared with the t_{MP} sampled in the previous MPPT cycle. The comparison reveals the input power change of two consecutive MPPT cycles based on Eq. (5), as V_{OUT} is hardly changed between the short sampling time intervals. If the t_{MP} of this MPPT cycle is larger than the previous cycle, it means that input power grows up in this cycle. Then the movement direction of R_{eq} is the same as the previous cycle; otherwise, the circuit changes the movement direction of R_{eq}.

Therefore, the circuit gradually approaches the maximum power point(MPP) and hovers at three states closest to the MPP in the end. The three states are the point B, C, D in Figure 4.

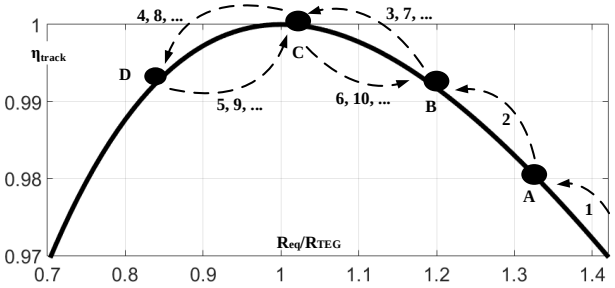

Figure 4. Process of the time exponential rate P&O algorithm.

Because of the high conversion rate ($t_{MN} \gg t_{MP}$), R_{eq} can be approximated to

$$R_{eq} = \frac{V_{TEG}}{\overline{I_L}} = \frac{2TL}{t_{MN}(t_{MN}+t_{MP})} \approx \frac{2TL}{t_{MN}^{2}} \tag{9}$$

According to Eq. (9), R_{eq} is inversely proportional to the square of the t_{MN}, and the function of exponential moving the R_{eq} is easy to implement by tuning the t_{MN} exponentially.

By adopting the time exponential rate P&O, the change rate of the perturbation can be set properly neither too small to distinguish the power change nor too large to reduce the tracking efficiency for various R_{TEG}. The MPPT circuit achieves an enhanced tracking efficiency for a wide internal resistance range of TEG. Meanwhile, the circuit observes and perturbs power according to the power transistor on-time, which greatly simplifies the circuit.

3. Circuit implementation

The architecture of the proposed MPPT circuit based on the time exponential rate P&O is shown in Figure 5, including a zero current detection (ZCD), a power modulator (PM), a time sensor, an oscillator (OSC), and power transistor drivers (Ndriver, Pdriver). The boost converter works in PWM mode. ZCD predicts when reverse current occurs on the inductor, and then turns off MP by signal GP_OFF and outputs digital signal TP<8:0> to represent the length of time t_{MP}. According to the time exponential rate P&O, the power modulator compares the TP<8:0> of two consecutive MPPT cycles to obtain the input power change and then generates a pulse width modulating signal (V_{PMO}) to adjust t_{MN}. Time sensor converts the MN on-time to voltage V_{ON}. Once V_{ON} reaches V_{PMO}, the output of the comparator resets the following D flip-flop, thereby defining t_{MN}.

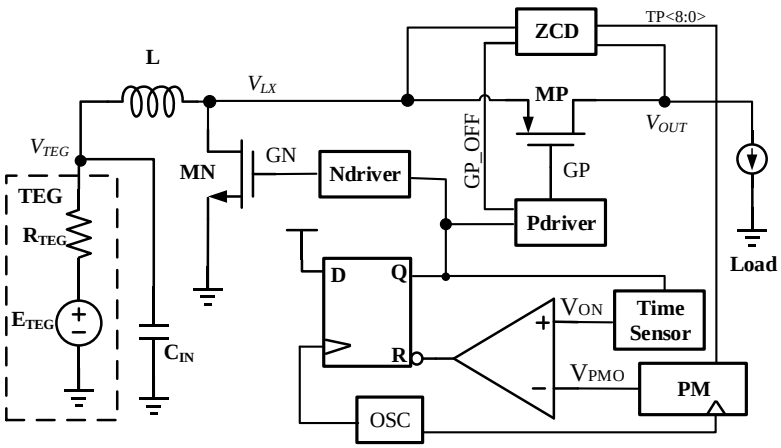

Figure 5. The architecture of the proposed MPPT circuit.

3.1 Predictive zero current detection

According to the time exponential rate P&O algorithm, the power change is obtained by comparing the MP on-time. Therefore, a high-precision ZCD is crucial.

When the ZCD turns off MP slowly, a reverse current appears on the inductor for a time, as shown in Figure 6(a). Because the drain-substrate PN junction of the MN forms a discharge path of the reverse current, the voltage at the right end of the inductor (V_{LX}) will first fall to the negative PN junction voltage ($-V_D$). When the ZCD turns off MP quickly, a little forward current remains on the inductor, as shown in Figure 6(b). The forward current flows through the source-substrate PN junction of the MP. Therefore, the V_{LX} will first jump to the sum of the substrate voltage and the PN junction voltage ($V_{OUT}+V_D$).

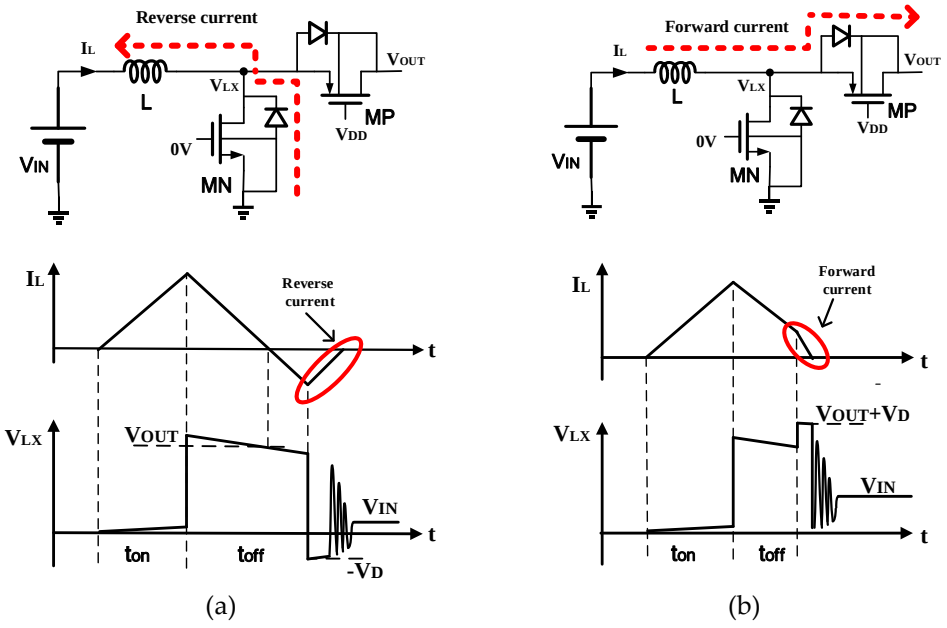

Figure 6. the discharge path of remaining current and waveforms after the MP is turned off (a) slowly (b) quickly

Based on the above analysis, there are two different situations of the V_{LX} after the MP is turned off, and a predictive ZCD is proposed as shown in Figure 7. When the MP is turned on, current source I1 starts to charge capacitor C1. Until V_{C1} is higher than V_{TP}, DFF is set by the COM1 and the ZCD output signal GP_OFF turns off the MP. In each converter cycle, after the MP is turned off, V_{LX} compares with $V_{OUT}/2$ by a dynamic comparator COM2. Then the 9-bit bidirectional counter (BDC) is triggered to read the result of the COM2. If the BDC input DIR is high, the BDC output TP<8:0> plus one. Otherwise, the TP<8:0> minus one. The TPn<8:0> is used to control whether a series of proportional current mirrors are connected to resistor R2, which defines V_{TP}.

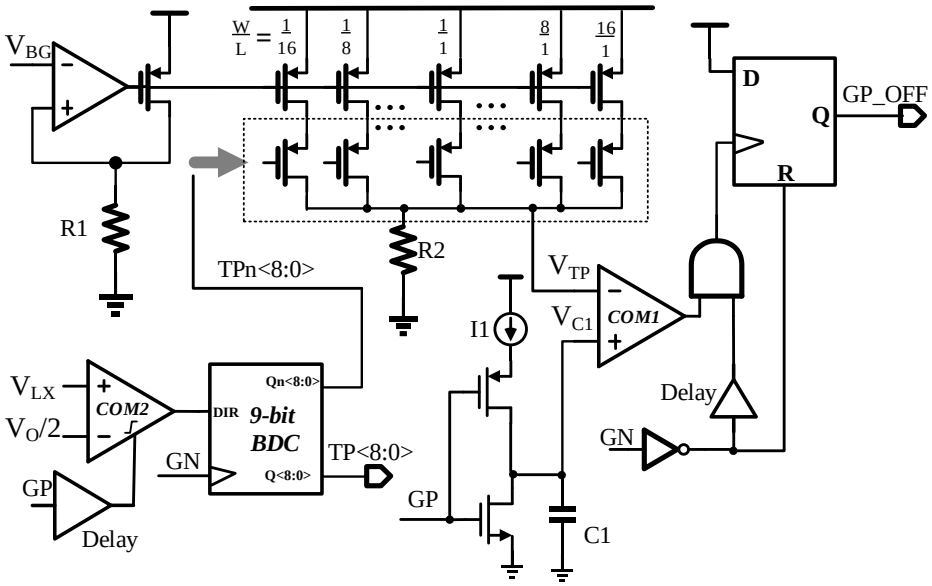

Figure 7. Predictive zero current detection

When V_{LX} is higher than $V_{OUT}/2$, which means the MP is turned off early in this cycle, TP<8:0> and V_{TP} will increase and the MP will be shut down later in the next cycle, and vice versa. Therefore, the predictive ZCD continuously corrects the TP<8:0> in each cycle and the t_{MP} is set around the best turn-off time adaptively. Consequently, the high-precision predictive ZCD is achieved. Meanwhile, the digital output TP<8:0> can be handled easily by the following circuit.

3.2 Time exponential rate power modulator

According to the time exponential rate P&O algorithm in section 2, a proposed power modulator observes the power change by comparing TP<8:0> and provides the control signal V_{PMO} to change the length of time t_{MN}, as shown in Figure 8. The input control signals CLK_TP, CLK_TN, CLK_SAV come from OSC and are used to execute the power modulator sequentially, as shown in Figure 8(b). Generally, an MPPT cycle, during which the circuit changes t_{MN} once, includes dozens of DC-DC converter cycles to ensure that the circuit reaches a stable state again.

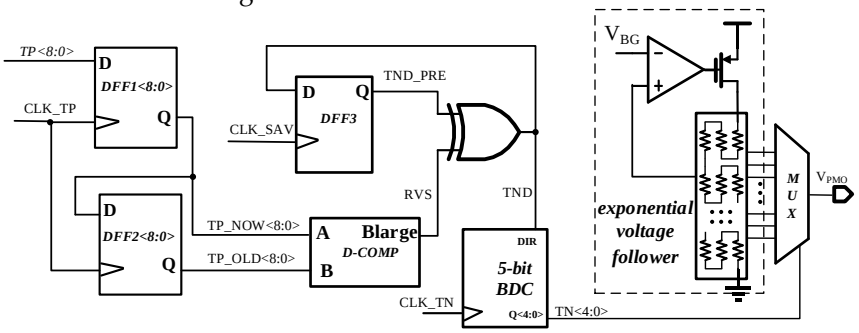

(a)

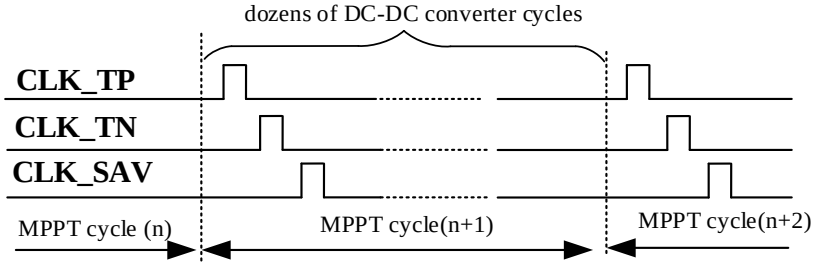

(b)

Figure 8. Time exponential rate power modulator (a) schematic (b) input control signal

At the beginning of each MPPT cycle, two groups of flip-flops (DFF1<8:0>, DFF2<8:0>) are triggered to save the present and previous time-length values TP<8:0>. After that, a digital comparator (D-COMP) compares these two values, and output a high level when the previous one is larger. And then, the D-COMP output (RVS) and the previous moving direction of t_{MN} (TND_PRE) do XOR operation. If RVS is low, the present moving direction (TND) is set to equal to the previous. If not, TND will be reversed. According to TND, signal TN<4:0> will plus or minus one by 5-bit BDC when the pulse CLK_TN arrives. An exponential voltage follower consists of an amplifier, a transistor, and a series of resistors, and outputs a series of voltages, which grows exponentially. According to TN<4:0>, the output of the power modulator (V_{PMO}) increases or decreases exponentially in each MPPT cycle by the multiplexer (MUX) and the voltage follower. Finally, the DFF3 is triggered to save TND for calculation in the next MPPT cycle.

4. Simulation Results

The proposed MPPT circuit using the time exponential rate P&O algorithm for TEG is implemented and simulated with a 110nm standard CMOS process. The total silicon chip occupies an area of 1.5 mm^2 (with pads), as shown in Figure 9.

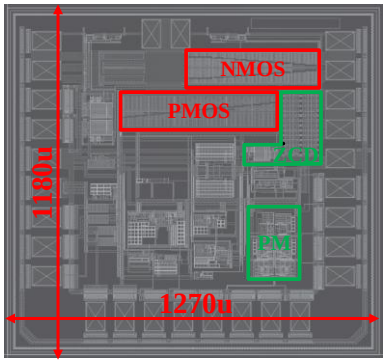

Figure 9. Layout view of the proposed MPPT circuit

A voltage source E_{TEG} and a resistance R_{TEG} are connected in series to mimic the TEG. Figure 10 displays the simulation waveform of the TEG output voltage V_{TEG} when E_{TEG} changes from 50mV to 400mV and R_{TEG} is 6Ω. As described in section 2, V_{TEG} oscillates in three states closest to $E_{TEG}/2$, which is the maximum power point.

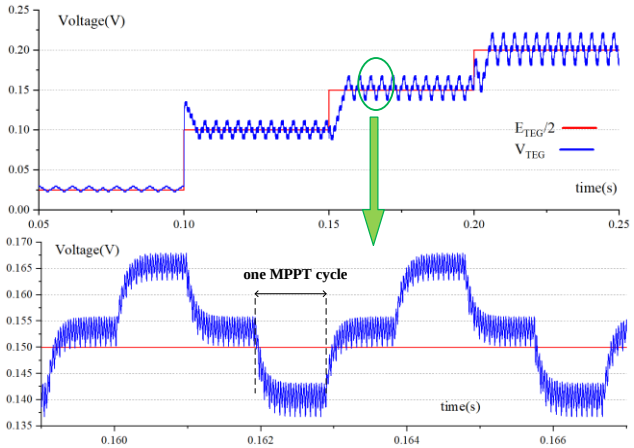

Figure 10. The waveform of V_{TEG}, when E_{TEG} changes from 50mV to 400mV and R_{TEG} is 6Ω.

The simulation result of the tracking efficiencies of the proposed MPPT circuit is between 98.9% and 99.5% for E_{TEG} from 50mV to 400mV and R_{TEG} from 1Ω to 12Ω, as shown in Figure 11, indicating that the MPPT circuit maintains extremely high tracking efficiency in a wide TEG range.

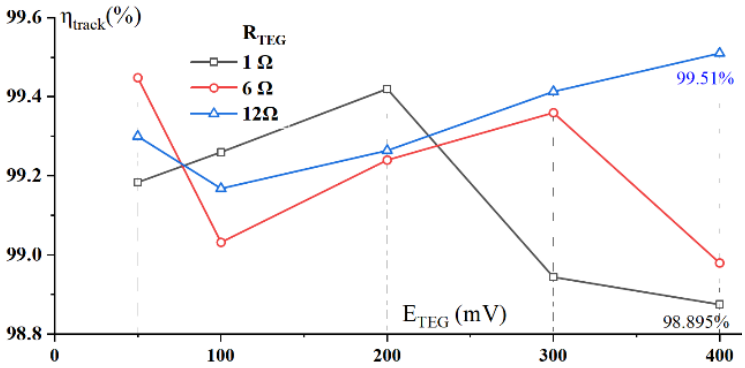

Figure 11. Tracking efficiencies of the proposed circuit at different conditions

For comparison, Figure 12 illustrates the tracking efficiencies of the compared MPPT circuit, which realizes P&O technology by fixed time step length perturbing. With the increase of R_{TEG}, the perturbation of t_{MN} should be smaller to keep the same tracking efficiency. Therefore, the η_{track} of the long time step circuit gradually decrease from 98.7% to 92.3%. However, when the fixed time step length is set short, the change of power is too small to be observed correctly at low R_{TEG}. Therefore, the circuit will oscillate before reaching the MPP. Then, the η_{track} keeps a high level at high R_{TEG} and decreases significantly at low R_{TEG}, as shown in Figure 12. Comparing with the fixed time step P&O scheme, the proposed time exponential rate P&O scheme keeps high tracking efficiency in a wider R_{TEG} range.

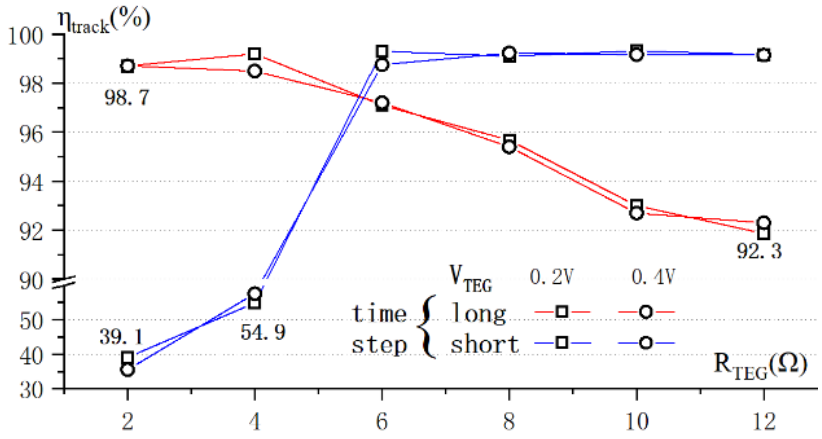

Figure 12. Tracking efficiencies of the compared MPPT circuit with a fixed time step P&O scheme

Table 1 shows a comparison of this work with other state-of-the-art MPPT techniques for TEG. Previous MPPT circuit with the FOCV technique by Luo [20] achieves peak tracking efficiencies of 96%, but he only utilizes TEG with fixed internal resistance and doesn't probe into the influence of internal resistances on tracking efficiency. Shrivastava [21] tested different internal resistances, and the tracking efficiency decreases 7% when the internal resistance varies from 5 to 10Ω. Moreover, the FOCV technique must frequently stop the boost circuit for a while to sample the open-circuit voltage, which reduces the system efficiency. Comparing with previous works using the P&Q technique [22, 23], the proposed MPPT circuit using time exponential rate P&O technique keeps tracking efficiency at a high level from 98.9 to 99.5%, and the applicable range of the TEG resistance is from 1 to 12Ω, which is enhanced at least 2.2 times.

Table 1. Performance comparisons with related works

	TCASI '18 [20]	JSSC '15 [21]	TCASI '17 [22]	JSSC '12 [23]	This work
Process	65nm	130nm	65nm	0.35um	110nm
Energy Source	thermal	thermal &solar	thermal &solar	thermal &solar &vibration	thermal
Tracking efficiency	<96%*	92-99%	83-96.2%	<96%	98.9-99.5%
Input voltage	15-240mV	20-300mV (TEG)	0.4-1.7V	20-160mV (TEG)	50-400mV
TEG Resistor	5Ω	5~10Ω	NA	5~10Ω	1~12Ω
MPPT method	FOCV	FOCV	P&O	P&O	P&O

note*: calculated with end-to-end efficiency divided by conversion efficiency

5. Conclusions and Discussions

The time exponential rate P&O technology is proposed in this work to extract the maximum electrical energy from TEG. By using the time exponential rate P&O, the proposed MPPT circuit observes the power change by comparing PMOS on-time and perturbs the power by adjusting NMOS on-time exponentially, which shows an enhanced tracking efficiency for a wide range of TEG. The MPPT circuit is implemented in a 110nm CMOS process and its tracking efficiencies vary from 98.9% to 99.5% with TEG open-circuit voltage from 50mV to 400mV and the TEG internal resistance from 1Ω to 12Ω.

This time exponential rate P&O technology is expected to contribute to the versatility of the MPPT circuit for various TEGs, which are made of varied semiconductor materials and have different internal resistances. However, there are also limitations of the proposed MPPT circuit. Nowadays, a multiple-input multiple-output (MIMO) converter is a trend for energy harvester. The MIMO converter can store partial electricity when the ambient energy is redundant, and this electricity can be used to power the load when the ambient energy is insufficient. However, the proposed MPPT circuit is designed for single input single output (SISO) system. The time exponential rate P&O technology should be reconsidered for the MIMO system, especially when the voltage of the electricity storage capacitor (V_{ST}) is low, and the high conversion rate ($V_{ST} \gg V_{TEG}$) is impossible. These challenges will become our important future research direction of the MPPT circuit.

Author Contributions: Conceptualization, H.C. and J.M.; methodology, J.M. and H.C; investigation, J.M.; data curation, J.M. and Y.L.; project administration, W.L.; funding acquisition, Z.S. and Y.L. All authors have read and agreed to the published version of the manuscript.

Funding: This research was funded by the National Key Research and Development Program of China (2017YFB0701703, 2017YFA0206104, 2017YFB0405601, 2018YFB0407500), National Natural Science Foundation of China (61874178, 61874129, 91964204, 61904186, 61904189), Strategic Priority Research Program of the Chinese Academy of Sciences (XDB44010200), Science and Technology Council of Shanghai (17DZ2291300, 19JC1416801), Shanghai Sailing Program (19YF1456100).

Institutional Review Board Statement: Not applicable.

Informed Consent Statement: Not applicable.

Data Availability Statement: Not applicable.

Acknowledgments: The authors would thank the Semiconductor Manufacturing International Corporation (SMIC) for support.

Conflicts of Interest: The authors declare no conflict of interest.

References

1. Said, O.; Albagory, Y.; Nofal, M.; Raddady, F.A. IoT-RTP and IoT-RTCP: Adaptive Protocols for Multimedia Transmission over Internet of Things Environments. *IEEE Access* **2017**, *5*, 16757-16773, doi:10.1109/ACCESS.2017.2726902.

2. Wang, Y.; Gawryszewska-Wilczynsk, P.; Zhang, X.; Yin, J.; Wen, Y.; Li, H. Photovoltaic efficiency enhancement of polycrystalline silicon solar cells by a highly stable luminescent film. *Science China Materials* **2020**, *63*, 544-551, doi:10.1007/s40843-019-1246-5.
3. Meneghello, F.; Calore, M.; Zucchetto, D.; Polese, M.; Zanella, A. IoT: Internet of Threats? A Survey of Practical Security Vulnerabilities in Real IoT Devices. *IEEE Internet of Things Journal* **2019**, *6*, 8182-8201, doi:10.1109/JIOT.2019.2935189.
4. Chen, I.C.; Liang, C.W.; Tsai, T.H. A Single-Inductor Dual-Input Dual-Output DC–DC Converter for Photovoltaic and Piezoelectric Energy Harvesting Systems. *IEEE Transactions on Circuits and Systems II: Express Briefs* **2019**, *66*, 1763-1767, doi:10.1109/TCSII.2019.2921349.
5. Chen, P.H.; Cheng, H.C.; Lo, C.L. A Single-Inductor Triple-Source Quad-Mode Energy-Harvesting Interface With Automatic Source Selection and Reversely Polarized Energy Recycling. *IEEE Journal of Solid-State Circuits* **2019**, *54*, 2671-2679, doi:10.1109/JSSC.2019.2917549.
6. Muñoz, R.; Vilalta, R.; Yoshikane, N.; Casellas, R.; Martínez, R.; Tsuritani, T.; Morita, I. Integration of IoT, Transport SDN, and Edge/Cloud Computing for Dynamic Distribution of IoT Analytics and Efficient Use of Network Resources. *Journal of Lightwave Technology* **2018**, *36*, 1420-1428, doi:10.1109/JLT.2018.2800660.
7. Jaziri, N.; Boughamoura, A.; Müller, J.; Mezghani, B.; Tounsi, F.; Ismail, M. A comprehensive review of Thermoelectric Generators: Technologies and common applications. *Energy Reports* **2020**, *6*, 264-287, doi: 10.1016/j.egyr.2019.12.011.
8. Watson, T.C.; Vincent, J.N.; Lee, H. Effect of DC-DC voltage step-up converter impedance on thermoelectric energy harvester system design strategy. *Applied Energy* **2019**, *239*, 898-907, doi: 10.1016/j.apenergy.2019.02.005.
9. Verma, G.; Sharma, V. A Novel Thermoelectric Energy Harvester for Wireless Sensor Network Application. *IEEE Transactions on Industrial Electronics* **2019**, *66*, 3530-3538, doi:10.1109/TIE.2018.2863190.
10. Coustans, M.; Krummenacher, F.; Kayal, M. A Fully Integrated 60 mV Cold-Start Circuit for Single Coil DC–DC Boost Converter for Thermoelectric Energy Harvesting. *IEEE Transactions on Circuits and Systems II: Express Briefs* **2019**, *66*, 1668-1672, doi:10.1109/TCSII.2019.2922683.
11. Lim, B.; Seo, J.; Lee, S. A Colpitts Oscillator-Based Self-Starting Boost Converter for Thermoelectric Energy Harvesting With 40-mV Startup Voltage and 75% Maximum Efficiency. *IEEE Journal of Solid-State Circuits* **2018**, *53*, 3293-3302, doi:10.1109/JSSC.2018.2863951.
12. Bassi, G.; Colalongo, L.; Richelli, A.; Kovacs-Vajna, Z.M. 100 mV–1.2 V fully-integrated DC–DC converters for thermal energy harvesting. *Iet Power Electronics* **2013**, *6*, 1151-1156, doi:10.1049/iet-pel.2012.0625.
13. Tellurex. Tellurex Thermoelectric Energy Harvester-G1-1.0-127-1.27, **2011**, http://educypedia.karadimov.info/library/termo.pdf
14. C. J. Cauchy et al.: U.S. Patent 6103967, **2000**.
15. Shim, M.; Kim, J.; Jeong, J.; Park, S.; Kim, C. Self-Powered 30 μW to 10 mW Piezoelectric Energy Harvesting System With 9.09 ms/V Maximum Power Point Tracking Time. *IEEE Journal of Solid-State Circuits* **2015**, *50*, 2367-2379, doi:10.1109/JSSC.2015.2456880.
16. Leoni, A.; Pantoli, L. SPICE Model Identification Technique of a Cheap Thermoelectric Cell Applied to DC/DC Design with MPPT Algorithm for Low-Cost, Low-Power Energy Harvesting. *Applied Sciences* **2019**, *9*, doi:10.3390/app9183744.
17. Vaisband, I.; Saadat, M.; Murmann, B. A Closed-Loop Reconfigurable Switched-Capacitor DC-DC Converter for Sub-mW Energy Harvesting Applications. *IEEE Transactions on Circuits and Systems I: Regular Papers* **2015**, *62*, 385-394, doi:10.1109/TCSI.2014.2362971.
18. Teh, Y.; Mok, P.K.T. Design of Transformer-Based Boost Converter for High Internal Resistance Energy Harvesting Sources With 21 mV Self-Startup Voltage and 74% Power Efficiency. *IEEE Journal of Solid-State Circuits* **2014**, *49*, 2694-2704, doi:10.1109/JSSC.2014.2354645.
19. M'zoughi, F.; Garrido, I.; Garrido, A.J.; De La Sen, M. Rotational Speed Control Using ANN-Based MPPT for OWC Based on Surface Elevation Measurements. *Applied Sciences* **2020**, *10*, doi:10.3390/app10248975.
20. Luo, Z.; Zeng, L.; Lau, B.; Lian, Y.; Heng, C. A Sub-10 mV Power Converter With Fully Integrated Self-Start, MPPT, and ZCS Control for Thermoelectric Energy Harvesting. *IEEE Transactions on Circuits and Systems I: Regular Papers* **2018**, *65*, 1744-1757, doi:10.1109/TCSI.2017.2757505.
21. Shrivastava, A.; Roberts, N.E.; Khan, O.U.; Wentzloff, D.D.; Calhoun, B.H. A 10 mV-Input Boost Converter With Inductor Peak Current Control and Zero Detection for Thermoelectric and Solar Energy Harvesting With 220 mV Cold-Start and -14.5 dBm, 915 MHz RF Kick-Start. *IEEE Journal of Solid-State Circuits* **2015**, *50*, 1820-1832, doi:10.1109/JSSC.2015.2412952.
22. Rawy, K.; Kalathiparambil, F.; Maurath, D.; Kim, T.T. A Self-Adaptive Time-Based MPPT With 96.2% Tracking Efficiency and a Wide Tracking Range of 10 uA to 1 mA for IoT Applications. *IEEE Transactions on Circuits and Systems I: Regular Papers* **2017**, *64*, 2334-2345, doi:10.1109/TCSI.2017.2693405.
23. Bandyopadhyay, S.; Chandrakasan, A.P. Platform Architecture for Solar, Thermal, and Vibration Energy Combining With MPPT and Single Inductor. *IEEE Journal of Solid-State Circuits* **2012**, *47*, 2199-2215, doi:10.1109/JSSC.2012.2197239.